Cluster and Solute Velocity Distributions in Free-Jet Expansions of Supercritical CO_2

Silvia De Dea,[†] David R. Miller,*[,†] and Robert E. Continetti*[,‡]

Department of Mechanical and Aerospace Engineering and Department of Chemistry and Biochemistry, University of California, San Diego, 9500 Gilman Drive, La Jolla, California 92093-0001

Received: June 25, 2008; Revised Manuscript Received: October 23, 2008

The free-jet expansions of high-pressure CO_2 supercritical solutions are probed by direct sampling mass spectrometry. Both cluster intensity measurements and velocity distribution measurements are reported for expansions which result in cluster formation by condensation and fragmentation of supersaturated vapors and superheated liquids. The resulting velocity distributions for these highly nonequilibrated expansions are characterized by up to three different peaks, depending on the source conditions: two primary peaks associated with very large clusters, the slower of which is associated with liquid fragmentation, and a smaller faster peak associated with monomers and small CO_2 clusters. We have associated the slow peak, observed only for fragmentation of superheated liquid expansions, with a liquid or condensed phase fragment by measuring the velocity distribution of low vapor pressure solutes in the expansion of supercritical CO_2 mixtures.

1. Introduction

We have recently used free-jet expansions of a binary mixture of ferric acetylacetonate, $Fe(acac)_3$, in supercritical CO_2, at 140 bar and 343 K, to grow thin magnetically ordered films on silicon substrates.[1,2] The high-pressure solutions are rapidly decompressed by expanding to atmospheric or vacuum conditions through small apertures. The solutes precipitate out in the expansion and the resulting jet flow is directed onto a substrate where film growth occurs. This process has widespread application and is referred to as RESS (Rapid Expansion of Supercritical Solutions).[3−5] To understand the characteristics of the fluid that impacts the substrate it was decided to interface the RESS nozzle source directly to a molecular beam apparatus and sample the free-jet expansion with mass spectrometer systems, capable of identifying the species present and their translational energies. This is a well-established research area called direct-sampling mass spectrometry (DSMS) and was previously used in our laboratories to sample and characterize the chemistry in a supercritical water reactor.[6] In this paper we report cluster measurements and cluster velocity distribution measurements for expansions of pure supercritical CO_2, and for RESS expansions of CO_2/$Fe(acac)_3$ and CO_2/naphthalene supercritical solutions. We find the degree of nonequilibrated velocity slip between the various species which persists in the high-density continuum flow free-jet expansions to be remarkable and related to the molecular dynamics of the clustering and fragmentation processes.

Clustering and nonequilibrium relaxation kinetics in free-jet expansions have been studied widely by researchers.[7−17] The resulting expansion properties are very sensitive to the particular conditions used in each laboratory, especially nozzle geometry and initial stagnation conditions, which makes it difficult to compare quantitatively one study with another, especially for the expansion of nonideal gases like supercritical CO_2. With respect to high-pressure supercritical CO_2, researchers have characterized similar expansions by Raman and Rayleigh scattering,[18] by FTIR spectroscopy,[19] and by pulsed electron beam time-of-flight velocity measurements.[20] While we will comment on their results compared to ours, the advantage of the molecular beam based mass spectrometer is the ability to monitor simultaneously many species at high sensitivities and to be coupled to a time-of-flight velocity distribution measurement. Only a few groups have attempted to detect nonvolatile solutes by coupling pulsed CO_2 expansions to a DSMS system.[20,21] To our knowledge, this is the first use of DSMS to characterize clusters and solutes, especially their velocities, in continuous supercritical CO_2 and CO_2−solute expansions.

All of the expansions studied here are into vacuum background pressures so that there are no strong continuum shock waves present, which occur for RESS expansions into atmospheric background pressures.[8−10,22,23] However, even at these low pressures there can be substantial collisions with molecules which reflect from the chamber surfaces and with background gases, which requires care in sampling the expansions as described below. The expansions are adiabatic and have been observed to often follow closely to an isentropic expansion because the expansions are supersonic and any molecular viscous or heat transfer processes are of second order. These expansions are not isenthalpic because of the high supersonic speeds in which most of the initial enthalpy at source stagnation conditions is converted into mean kinetic energy.[8] We therefore find it useful to describe and visualize the expansion trajectories on a $T-S$ diagram. At supercritical conditions the CO_2 is highly nonideal, the residual enthalpy is negative, and an ideal gas model is inadequate.[2,6,22−24] Khalil's recent computations and experiments have suggested that the Peng−Robinson equation of state (PR-EOS) is a good approximation for supercritical CO_2 expansions.[22] We therefore show a $T-S$ diagram in Figure 1 based on the PR-EOS. Vertical expansion trajectories are indicated for a vapor free-jet RESS expansion, with stagnation conditions $T_o = 343$ K and $P_o = 140$ bar and for a liquid free-jet RESS expansion, with stagnation conditions $T_o = 323$ K and $P_o = 140$ bar, identical to those used in our film growth experiments and investigated here by DSMS. A more rigorous equation of state is the Helmholtz energy formulation of Span

* Corresponding author. D.R.M.: phone +18585343131, fax +18585345355, e-mail: dmiller@ucsd.edu, rcontinetti@ucsd.edu. R.E.C.: phone +18585345559, fax +18585349856.
[†] Department of Mechanical and Aerospace Engineering.
[‡] Department of Chemistry and Biochemistry.

10.1021/jp805618z CCC: $40.75
Published on Web 12/19/2008

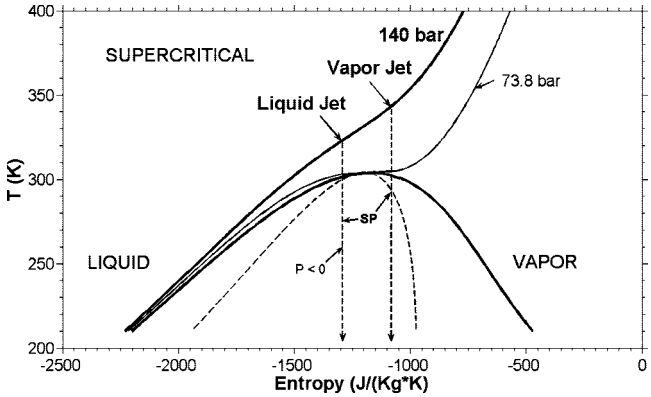

Figure 1. $T-S$ diagram calculated for CO_2 with the Peng−Robinson equation of state including the thermodynamic spinodal (dotted line). Vapor free-jet (T_o = 343 K, P_o = 140 bar) and liquid free-jet (T_o = 323 K, P_o = 140 bar) isentropic trajectories are indicated for the adiabatic RESS expansion on which the predicted sonic points (SP) are indicated. For the liquid jet the hypothetical expansion point where negative pressures would be predicted to occur is also indicated (see text for discussion).

and Wagner, involving a 42-term expansion,[25] but we find that the PR-EOS compares reasonably well and it can be extended further into the two-phase region to predict metastable conditions. The vertical trajectories indicated on the $T-S$ diagram represent a limit and the trajectories will bend to larger entropies as the expansion proceeds and there are substantial nonequilibrium kinetic effects, such as rapid nucleation or fragmentation.

What we call the vapor jet enters the two-phase region on the vapor side of the critical point while the liquid jet enters on the liquid side. It is expected that the clustering and energy distributions will be different for these two types of expansions because vapor jets become highly supersaturated and form small clusters through kinetic clustering processes, while liquid jets become highly superheated and form vapor and particle fragment products by nonequilibrium fragmentation.[12,26] However, both processes are limited thermodynamically to saturated vapor and liquid or solid state phases. For the rapid RESS expansions of the current study, which occur on microsecond time scales and expand to low densities, classical nucleation or bubble formation models may not apply because of limited molecular collisions and associated energy transfer. Indicated on the $T-S$ diagram are the thermodynamic spinodal curve based on the PR-EOS, the sonic points (SP) where the flows would be predicted by the PR-EOS to reach Mach number = 1 at the throat or exit of the nozzle, and, for the liquid free-jet, the point at which the fluid would be subjected to negative pressures. The latter two points are hypothetical since they represent unstable, nonequilibrium states beyond the spinodal points in the expansions when we can expect substantial clustering and fragmentation.[27,28]

The liquid jet expansions studied here have implications for molecular dynamics simulations of the rapid fragmentation of superheated liquids, an area that has received considerable investigation experimentally and theoretically since the early 1960s.[26−33] The type of hydrodynamic fragmentation processes which balance pressure and surface tension forces and fragment kinetic energies[27,29,30,34] should be particularly relevant for these RESS expansions.

In the sections below, we briefly describe the DSMS apparatus in which both a time-of-flight (TOF) mass spectrometer and quadrupole mass spectrometers (QMS) are used. We also describe a time-of-flight velocity distribution measurement, referred to as "tof" to distinguish it from the "TOF" mass spectrometer. The techniques are standard in the molecular beam community and complete details of the apparatus and procedures are available elsewhere.[2] Experimental data for the cluster distributions are only briefly summarized while more detailed data are presented for the velocity distributions obtained in the RESS expansions. While we do not fully understand the underlying molecular mechanisms which yield the velocity results, we provide qualitative analyses for possible limiting factors.

2. Experimental Apparatus

The basic features of the apparatus are shown in Figure 2. The apparatus is a classical molecular beam system used by researchers for many decades and there is a rich literature on design parameters and the various techniques we use.[9,10,35] The serious caveats for such a DSMS system are sufficient vacuum pumping speeds to handle the very large mass flow rates and minimize background pressure effects on the expansion and sampling, the skimmer design to minimize beam interference and biasing of species, and the ionization of neutral beam species by electron bombardment in the mass spectrometer ionizer that causes fragmentation of the parent molecules.

The system is separated into three basic chambers, the source chamber pumped by a 110 L/s roots blower, followed by a buffer chamber evacuated by an Edwards 255 L/s turbomolecular pump and by a Balzers 230 L/s turbomolecular pump and a detection chamber, pumped by a 330 L/s Balzers turbomolecular pump, to house the QMS mass spectrometer; when the TOF mass spectrometer is used a fourth chamber, differentially pumped by a 170 L/s Balzers turbomolecular pump, is attached to extend the ion flight path to 1.7 m. Typical base pressures for the three chambers are 5×10^{-3}, 1×10^{-7}, 1×10^{-8} Torr, respectively, and under normal operating conditions background pressures reach 0.2, 1×10^{-5}, 1×10^{-7}, and 3×10^{-8} Torr in the TOF detector chamber. The high-pressure delivery system includes a CO_2 cylinder, a supercritical continuous pump, a heating bath, an extraction vessel, a bypass line, a UV−vis cell to monitor solute concentration, and the manipulator to hold and align the nozzle. For the present studies the nozzle is a 20 μm electron microscope aperture soldered to a stainless steel Swagelok cap. Stagnation temperature and pressure are measured in the supercritical fluid just upstream of the aperture in the stagnation chamber.

The RESS source chamber is separated from the buffer chamber by a sharp-edged, electroformed, conical nickel skimmer (Beam Dynamics, Inc.). For the high-pressure regime that we encounter in RESS experiments we relied on the classical research and design criteria of Campargue and colleagues.[8,35] The 0.3 mm diameter skimmer is 1.9 cm high and has an angle of 50° and a wall thickness of ~0.008 cm. A typical nozzle-to-skimmer distance was 4 mm or 200 nozzle diameters, which positioned the skimmer inside the Mach disk location.[8] The time-of-flight (tof) velocity distribution measurements are made by mechanically modulating the beam in the buffer chamber with a 12.7 cm diameter chopper wheel with four symmetric slits of width 0.1 mm. The chopper wheel is turned by a DC motor capable of rotational speeds up to 170 Hz. However, most of the data were taken at 50 Hz speeds as a tradeoff between velocity resolution and species sensitivity needed to make velocity measurements on clusters and solutes. The tof flight distance between the chopper and QMS ionizer, L = 79 cm, and chopper timing electronics were calibrated by measuring known terminal velocities for Ar and He free-jet expansions.

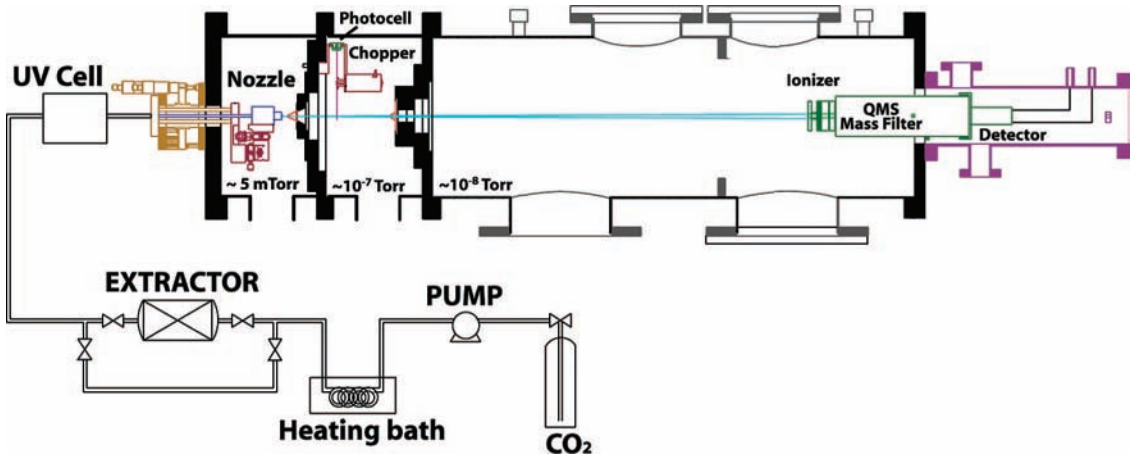

Figure 2. DSMS apparatus schematic diagram.

Time-of-flight (TOF) mass spectrometry is a well-known technique and many references are available that describe general theory and operating principles.[36,37] The TOF mass spectrometer adapted for our experiments, not shown in Figure 2, was previously developed for studies of matrix-assisted laser desorption ionization of metal oxides and proteins,[38] capable of detecting masses up to 20 000 amu. In our experiments, a resolution $m/\Delta m = 430$ was achieved for the CO_2 monomer signal ($m = 44$ amu) and a resolution $m/\Delta m = 890$ was achieved near mass 1300 amu.

Two different commercial quadrupole mass spectrometers have been used in the detector chamber, a Balzers QMS 311 and a rebuilt Extrel (270-9) mass spectrometer. While better resolution for the tof velocity measurements was achieved with the Balzers, because of its smaller ionizer, most of the data were collected with the Extrel because it was equipped with an improved detector and designed to span a wider mass range to 480 amu with better sensitivity. The electron multipliers for both spectrometers were mounted off-axis to discriminate against metastable species which may pass through the quadrupole field filters. The QMS does not have the mass range of the TOF mass spectrometer, but it is capable of much better species sensitivity using modulated beam detection and lock-in amplifier detection electronics, and it is easily used for the tof velocity distribution measurements. Cluster concentrations near 5 ppm were easily resolved and tof velocity data are reported below for $Fe(acac)_3$ solute concentrations near 100 ppm.

Since the RESS expansion is probed by the skimmer far out in the expansion, the effect of the expansion chamber background gas scattering, or penetration into the jet, can be important. Therefore, experiments were performed to study this effect by artificially increasing the pressure in the RESS expansion chamber while monitoring the CO_2 monomer signal for any changes. We artificially increased the background pressure, using Ar, by factors of 3−4 and observed no effect on the CO_2 beam signal, nor could we detect any Ar in the molecular beam. We concluded that the jet properties along the centerline to the skimmer, and the skimmer probing, were not affected significantly by the background gas pressure. Further, the high-density free-jet expansion was effective in protecting the subsequent molecular beam from background gas penetration.

Time-of-flight (tof) measurements of the translational velocity distribution in molecular beams formed by probing free-jets with conical skimmers have been studied and analyzed since the early 1960s.[9,11,39,40] We have assumed that the conventional drifting Maxwellian velocity distribution, $df(V) = [4/(\pi)^{1/2}]\text{-}[m/(2kT)]^{3/2}V^2 \exp[-m(V - V_o)^2/2kT]\, d(V)$, characterizes the velocity distribution of the fluid in the terminal state of the expansion at the skimmer tip. We used a numerical convolution to correct for the chopper gating effect and we extracted the mean velocity V_o and translational temperature T, or speed ratio $SR = V_o/(2kT/m)^{1/2}$ from the tof data. There are two serious caveats to our velocity distribution measurements: the skimming is not perfect due to molecular scattering from the skimmer external and internal walls, and we observe a substantial tail on the velocity tof distributions for the highest density species, which we feel is due to space charging effects in the ionizer of the QMS. These two effects are most serious for the reported speed ratios but not for the mean velocities. We feel our mean velocities are accurate to within 1% but that our reported speed ratios are less reliable due to the ionizer effects. Even so, our measured speed ratios lie between 8 and 39, and beam translational temperatures are typically a few degrees K, so that this inaccuracy on the width of the velocity distribution has little effect on the reported mean velocities and the overall energy balance for the CO_2 expansions studied here.

3. Experimental Results

In this report we present data only for the two expansions noted in Figure 1, the vapor jet ($P_o = 140$ bar, $T_o = 343$ K) and the liquid jet ($P_o = 140$ bar, $T_o = 323$ K). Other source conditions and more extensive results are presented elsewhere.[2]

3.A. Cluster Species. In addition to the complexities of kinetic clustering and fragmentation, a most serious caveat in all of these results is that the mass spectrometer detection uses electron bombardment to form the ions. This ionization process fragments the neutral species we are trying to characterize, so that quantitative assessment of species concentrations is not possible. We have not made any attempt to adjust our results for this effect, nor for others such as differential skimmer sampling and detector sensitivities for different masses.[8,11,28] For this reason we only briefly summarize qualitative aspects of our cluster concentration data before we report and discuss the more quantitative velocity distribution measurements.

Both liquid jet and vapor jet RESS expansions have been studied with the TOF-MS. CO_2 ion clusters were resolved up to $N = 40$, $(CO_2)^+_{40}$. We have not been able to detect the very large nanoscale clusters ($N > 10^5$) which are most likely present in both the vapor and liquid jet expansions, and which could contribute as well to the smaller cluster ion signals due to electron beam fragmentation. Figure 3 is a summary plot of the log of cluster ion signal (S_N) normalized by the CO_2

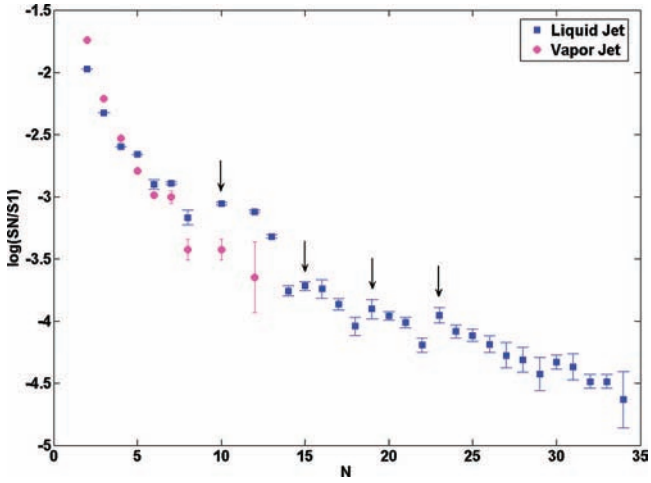

Figure 3. TOF mass spectrometer cluster distributions observed in the liquid jet (P_o = 140 bar, T_o = 323 K) and in the vapor jet (P_o = 140 bar, T_o = 343 K); arrows indicate observed maxima in the liquid jet distribution.

monomer ion signal (S_1), as a function of cluster size (N), for both the liquid and vapor jet. Cluster distributions in theoretical fragmentation studies[27,28,30,33] are often predicted to follow a logarithmic statistical distribution of cluster size. These TOF results for CO_2 clusters in both the liquid and vapor jets appear to show similar logarithmic distributions up to $N \approx 7$, but with a steeper slope below $N \approx 5$. Clusters above $N = 12$ are observed only in the liquid jet. The liquid jet cluster distribution also shows one clear maximum near $N = 10$, and several smaller maxima near $N = 15$, 19, and 23, which indicate a preferred configuration or "magic number".[41,42] The different cluster probability distributions found for the liquid and vapor jets, and especially for larger clusters in the liquid jet, are expected when comparing cluster formation from the condensation of a supersaturated vapor state (vapor jet) versus evaporation or fragmentation from the superheated liquid state (liquid jet).

The QMS mass spectrometer coupled with the lock-in amplifier has sensitivity several orders of magnitude higher than the TOF-MS, which permitted us to identify solute species of very low solubility. The main disadvantage of the QMS mass spectrometer that was available to us is a limited mass range (480 amu), so that only clusters up to $(CO_2)_{10}$ could be detected. We also made QMS measurements of solute species, including the weakly soluble $Fe(acac)_3$ (mole fraction $X_o \approx 10^{-4}$), in a liquid jet, and the highly soluble naphthalene in both liquid and vapor jets ($X_o \approx 10^{-2}$). Figure 4 is an example of a QMS spectrum for the $Fe(acac)_3/CO_2$ vapor jet, with fragments resolved below 100 ppm. As we show below, we have been able to make well-resolved tof velocity distribution measurements for these solutes, and for CO_2 clusters up to $N = 7$ in the vapor jet, and for the liquid jet up to $N = 8$. We were not able to detect any solute clusters or mixed solute−solvent clusters, or fragments that could be attributed to such clusters.

It is difficult to compare our species results with other researchers because clustering is very sensitive to stagnation conditions and nozzle geometry. Nevertheless we do wish to mention two studies that are relevant to ours. Bonnamy et al.[19] have used in situ FTIR measurements to characterize CO_2 expansions using a pulsed nozzle free-jet expansion. Their nozzles are larger (50 to 150 μm) than the ones used here and much of the reported data are for liquid CO_2 expansions from 400 bar and 298 K, which result in higher density jets than ours. On the basis of Mie scattering analysis and an assumed

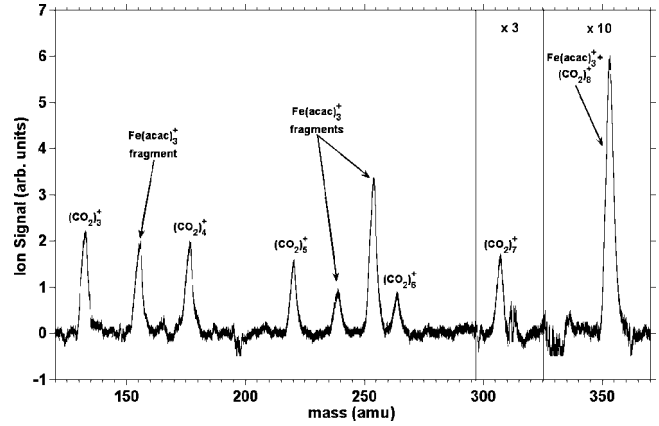

Figure 4. Ferric acetylacetonate QMS mass spectrum obtained from a supercritical $CO_2/Fe(acac)_3$ solution RESS expansion; P_o = 140 bar, T_o = 323 K, and $X_o = 1.5 \times 10^{-4}$.

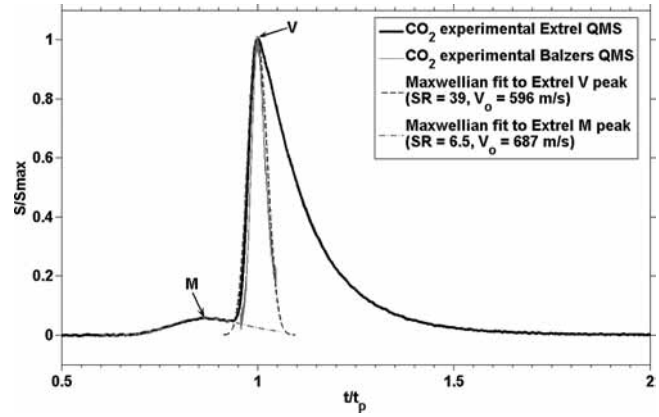

Figure 5. CO_2 monomer time-of-flight velocity distributions for a vapor free-jet RESS expansion (P_o = 140 bar, T_o = 343 K), obtained with the Extrel (black solid line) and Balzers (gray solid line) QMS. Data are normalized to the V peak and are shown together with the convoluted Maxwellian Gaussian fits to the Extrel data for the dominant V and faster M peaks (dotted lines).

log-normal size distribution, they report CO_2 clusters in the size range of order 100 nm for pure CO_2 expansions, corresponding approximately to $N \approx 10^7$. Bonnamy et al. also report measurements for phenanthrene and phytosterol solute clusters formed from liquid CO_2 expansions. They also cannot confirm any mixed clusters but feel their data support solute clusters coated by condensed CO_2. In another related study, Wodtke and Zhang[21] studied pulsed supersonic expansions of solutes dissolved in liquid CO_2. They coupled the RESS expansion with a time-of-flight mass spectrometer and studied expansions from 120 to 220 bar and 298 to 333 K using a 750 μm nozzle, much larger than our 20 μm nozzle. They studied expansions of solutes like caffeine, guanine, cholesterol, and mixed fullerenes obtaining similar spectra from both liquid and supercritical CO_2 expansions. They observed the formation of caffeine dimer only under high solute concentrations but again did not detect any solvent−solute mixed clusters.

3.B. CO_2 Vapor Jet Velocity Measurements. We present velocity time-of-flight data for the vapor jet and the liquid jet RESS expansions, first for pure supercritical CO_2, and then for expansions with solutes. Again, we will refer to the trajectories on the $T-S$ diagram, Figure 1, to identify and discuss these expansions.

Figure 5 shows a typical vapor jet CO_2^+ monomer ion tof spectrum taken with the Extrel QMS. Because of electron beam induced ion fragmentation in the mass spectrometer ionizer the

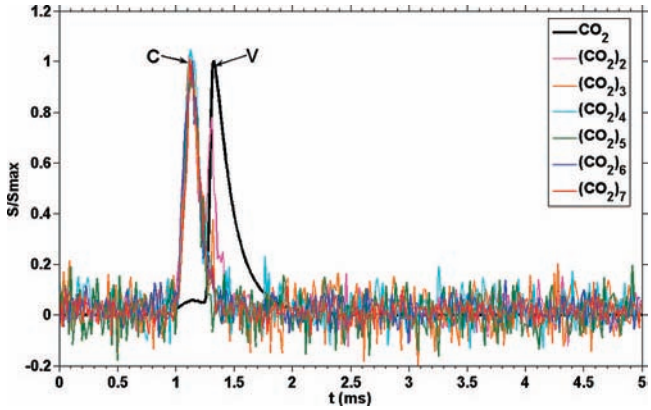

Figure 6. CO_2 monomer and cluster time-of-flight velocity distributions for a vapor free-jet RESS expansion ($P_o = 140$ bar, $T_o = 343$ K). Cluster spectra from $N = 2$ to 7 are indicated as the C peak.

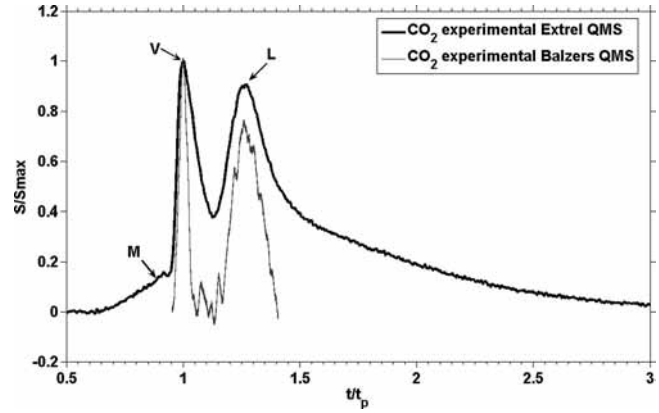

Figure 7. CO_2 monomer time-of-flight velocity distributions for a liquid free-jet RESS expansion ($P_o = 140$ bar, $T_o = 323$ K). Experimental data, normalized to the V peak, are shown for both the Extrel (black line) and Balzers (gray line) QMS.

monomer signal may be due either to monomer or to clusters of CO_2 in the expansion, discussed further below. The velocity distribution is characterized by two velocity peaks which indicate considerable velocity slip between species. For reasons that will become evident, we label these velocity peaks M for monomer and V for vapor. Also shown is a fit, deconvoluted for the chopper gating function, to the assumed drifting Maxwellian velocity distribution. The long tail at slow arrival times is evident and, as indicated, we have based our fits on the leading edge and peak of the distribution because we feel the tail in this case is primarily an artifact due to space charge in the commercial ionizer for these high-density beams. The dominant V peak has a velocity $V_p = 596$ m/s and speed ratio SR ≈ 39. To substantiate this treatment of the Extrel tof velocity data, we show in the same figure the tof distribution for this same expansion but made with the Balzers QMS, which has a much smaller ionizer and is better suited to the tof measurement. The Balzers tof data do not show the trailing edge and were fit to a SR ≈ 40, which compares well with the leading edge fit to the Extrel data. Since the Extrel was necessary to resolve the cluster and solute data given below, and because the monomer speed ratios are large and of secondary interest compared to the mean velocities, the data reported below are all taken with the Extrel QMS. As will be discussed below, we believe the V peak represents a distribution of very large condensed phase clusters formed in the vapor jet expansion which yield the strong monomer ion signal due to electron beam ionization fragmentation. The smaller, faster M peak, which we believe represents the primary monomer species, has a mean velocity of 687 m/s and can be fit with a SR ≈ 6.5.

We have been able to resolve tof data for clusters up to $N = 7$ in the vapor jet. Figure 6 shows all of the vapor jet cluster data, indicated by C, superimposed and compared with the monomer ion distribution; the cluster distributions can be fit with speed ratios between 15 and 20. The dimer distribution has two components, one aligned with the faster cluster C peaks and one aligned with the dominant V peak; we were not able to resolve a second slow peak for clusters above $N = 2$. There is clearly a great deal of velocity slip, and commensurate kinetic energies, between these smaller clusters and the primary V peak. We have not identified an experimental artifact to account for these velocity slip results and it appears to be substantiated by the dimer data, which indicates two well-resolved peaks, and by other results for solutes presented below. This anomalous velocity slip is one indication, discussed below, that the V peak represents very large condensed phase clusters which fragment when ionized to give the monomer ion signal. We note that the monomer under the C peak in Figure 6 appears small, which is due to the fact that the monomer signal has been scaled by the magnitude of the large V peak. On the basis of the actual detector sensitivities, the monomer is the dominant signal in the M and C peaks. The dimer is the largest cluster signal (see Figure 3) and is about 1% of the monomer in the M tof peak. In a related study, Christen and Rademann[43] have reported time-of-flight velocity distribution measurements for pure CO and CO_2 RESS type vapor jet expansions using a pulsed beam nozzle, in which they ionized the neutral species very near the nozzle exit. Because of the pulsed beam technique they were able to probe the jet very far out in the expansion, a nozzle-skimmer distance of 14.5 cm. Assuming the same Maxwellian velocity distribution, they report a mean CO_2 beam velocity of 686 m/s and CO_2 speed ratios of ~80 for source conditions $P_o = 74$ bar and $T_o = 322$ K. While their source conditions are at lower pressures, they use a conical nozzle with a much larger diameter of 300 μm so that one might expect much more clustering. They do not report any observation of multiple velocity peaks due to clusters. We have not observed the very high speed ratios they report, which could mean that we have some skimmer scattering interference, since our gating analysis suggests we could have resolved speed ratios as high as 100. The effect of ionizing the neutral beam in such a high density region so near the nozzle exit is not entirely clear, but the authors seem to have carefully considered this by reducing the number of ions formed to reduce any space charge effects. The other effect would be the artificially enhanced clustering due to ion-neutral collisions in the jet expansion, which could lead to substantial cluster formation, heavier masses, and therefore higher speed ratios for similar beam temperatures.

3.C. CO_2 Liquid Jet Velocity Measurements. Figure 7 shows a typical CO_2^+ liquid jet monomer tof spectrum, taken with the Extrel QMS and, as above, another taken with the Balzers QMS to again verify that the broad tail is likely an artifact of the larger Extrel ionizer. There are now three noticeable peaks, which we label M, V, and L. The faster M and V peaks correspond well with M and V peaks found for the vapor jet, adjusted for lower speeds due to the lower source temperature. Reported elsewhere,[2] we have tracked these two peaks and they move continuously from the vapor to the liquid side of the phase diagram, but as we pass through the critical point from vapor to liquid jets (see Figure 1) the new, slower L peak rapidly appears. We label it L because we feel it is associated with the very large condensed phase fragments which are generated when the superheated liquid undergoes rapid

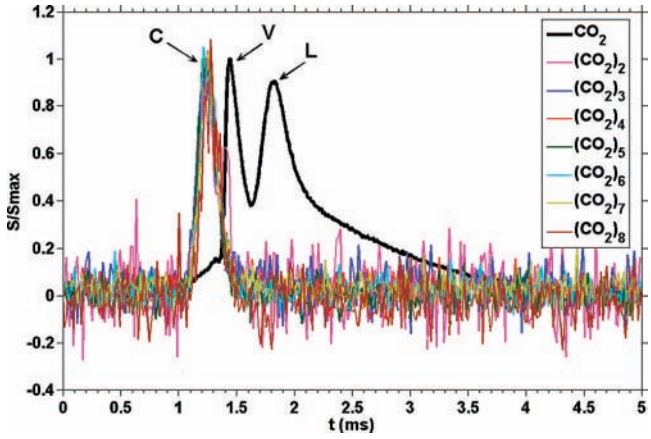

Figure 8. CO_2 monomer and cluster time-of-flight velocity distributions for a liquid free-jet RESS expansion (P_o = 140 bar, T_o = 343 K). Cluster spectra from N = 2 to 8 are indicated as the C peak.

fragmentation during the RESS expansion. This appearance of two dominant peaks for the liquid jet is analogous to that reported by Buchenau et al.,[31] who made similar measurements on supercritical liquid He jets. The mean velocities for M, V, and L species are ~630, 544, and 433 m/s respectively, which represent substantial differences in kinetic energies resulting from the formation and expansion of these fragmented species. The associated speed ratios are $SR_V \approx 32$ and $SR_L \approx 10$; the monomer M peak is not sufficiently resolved to estimate a speed ratio.

Figure 8 shows the time-of-flight velocity distributions of smaller clusters (C) formed in the liquid jet expansions, up to $N = 8$, again superimposed with the monomer species. As with the vapor jet it is very clear that all of the observed clusters are centered on the C peak. Although not clearly indicated here, the dimer again has a second component aligned with the V peak, but not with the L peak. The mean velocities for these clusters are centered on 627 ± 10 m/s and the speed ratios range between 12 and 22. As with the vapor jet expansions the differences in kinetic energy are substantial. The slow L peak is unique to the liquid jets and we have probed it further by introducing solutes into these RESS free-jet expansions.

3.D. CO_2/Solute Velocity Measurements. Naphthalene has excellent solubility in supercritical CO_2, with initial mole fraction of order $X_o \approx 0.01$, and therefore provides a good solute tag for the multiple velocity peaks we have observed in these RESS expansions. Figure 9 shows the velocity distribution for naphthalene expanded in a CO_2 vapor jet, again superimposed with the solvent monomer ion CO_2 distribution for reference. Naphthalene has nearly the same velocity and speed ratio as the principal V peak with V_o = 592 m/s, and a speed ratio SR = 33. Surprisingly, naphthalene does not have a velocity component commensurate with either the faster M peak, which has been attributed to the monomer fluid, or with the smaller clusters in the C peak. This result supports the QMS cluster data which did not indicate any small naphthalene clusters.

The velocity data for naphthalene in the liquid jet, Figure 10, show what is perhaps the most unique result of our studies to date: the solute is uniquely associated with the dominant L peak, the component that we ascribed to be associated with the liquid jet fragmentation. There is no evidence that the naphthalene solute molecule has a velocity component commensurate with the V, M, or C peaks; note that the mass of naphthalene is of the same order as $N = 3$ CO_2 clusters. Naphthalene in the liquid jet is characterized by $V_o \approx 423$ m/s, SR = 12. This finding suggests that when the liquid jet expands into the two-phase region, and subsequently fragments from a superheated liquid state, naphthalene has more affinity with the condensed liquid phase, a result consistent with its relatively low vapor pressure and discussed further below.

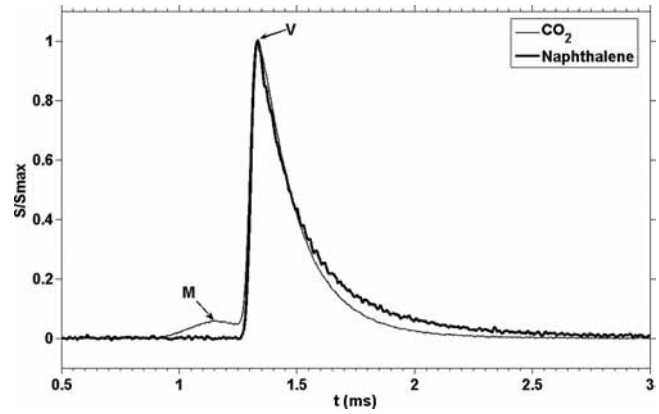

Figure 9. Time-of-flight velocity distribution for naphthalene expanded in a supercritical CO_2 vapor jet, superimposed with the solvent monomer CO_2 distribution; P_o = 140 bar, T_o = 343 K, $X_o \approx 0.01$.

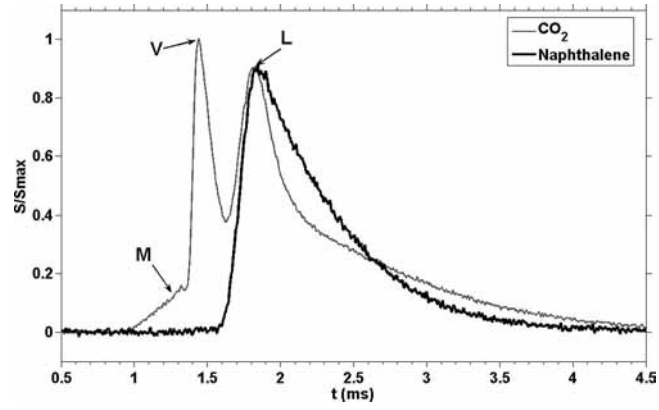

Figure 10. Time-of-flight velocity distribution for naphthalene expanded in a supercritical CO_2 liquid jet, superimposed with the solvent monomer CO_2 distribution; P_o = 140 bar, T_o = 323 K, $X_o \approx 0.008$.

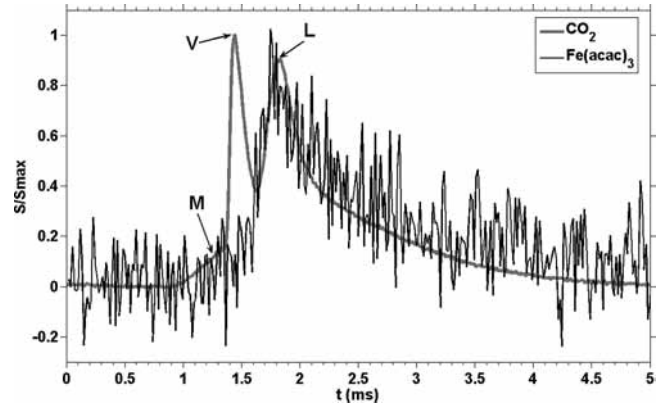

Figure 11. Time-of-flight velocity distribution for ferric acetylacetonate expanded in a supercritical CO_2 liquid jet, superimposed with the solvent monomer CO_2 distribution; P_o = 140 bar, T_o = 323 K, $X_o \approx 1.5 \times 10^{-4}$.

Figure 11 reflects the velocity distribution for the solute, the $Fe(acac)_3$ fragment at mass 255, expanded in the liquid CO_2 jet. $Fe(acac)_3$ has very low solubility ($X_o \approx 10^{-4}$) and again is associated with the L fragment peak. The $Fe(acac)_3$ solute velocity is characterized by $V_o \approx 435$ m/s, SR ≈ 8. The $Fe(acac)_3$ fragment at mass 155 was also detected and its velocity agreed well with this fragment at 255. We were not

able to measure the velocity of the parent solute ion because of the very weak signal.

In addition to naphthalene and $Fe(acac)_3$, we have also examined other ion fragmentation distributions from known parent molecules, in particular CO^+ formed from CO_2, in the QMS ionizer for both vapor and liquid jet expansions.[2] All of these known fragments gave identical tof distributions to the parent ion. We feel such results confirm that the multiple detected peaks and velocity slip are real and not artifacts due to the ionization fragmentation. Further, a reasonable estimate of the transit times within ionizer cannot account for the large delay times between the velocity peaks.

The striking result that the solutes, naphthalene, and $Fe(acac)_3$ both appear in only the L fragment peak can be addressed in part by asking whether these solutes would thermodynamically prefer to be in a liquid or in a vapor phase according to their molecular interactions as governed by, for example, the Peng−Robinson equation of state. A classical thermodynamic adiabatic flash point calculation[44] for the mixed solute−solvent fluid is useful for this purpose, which we have completed for the naphthalene/CO_2 systems. We chose the terminal flash conditions to be at the predicted thermodynamic spinodal point in the expansion. For our liquid jet expansion conditions we find that more than 99% of the naphthalene is predicted to be in the liquid phase of an equilibrium flash. This result would also support a hypothesis that the L peak is associated with large condensed phase particles formed in the fragmentation process from the superheated liquid expansion state.

In summary, for vapor jet expansions we observe a dominant peak, V, identified experimentally as monomer ions, preceded by faster monomer fluid, M, and small clusters, C, with mean speeds of order 15% higher; the associated differential kinetic energies are quite large depending on the cluster mass. The amount of velocity slip is unusual for such high density free-jets. When the expansion occurs on the liquid side of the phase space, the tof velocity analysis shows that the fragmentation process gives rise not only to the V, M, and C components, but also to a fourth slower component, which we associate with a condensed phase fragment. Again, the amount of slip between the L and V species is surprising (∼20%). Seeding solutes into the expansions clearly shows that the solutes remain in the L condensed phase following fragmentation of the superheated liquid expansions. We summarize our tof velocity data in Table 1, including data for both C and V dimer peaks; other data are reported elsewhere.[2] In addition to the monomer M peak, it is noted in the table where the CO_2 monomer data represent the V peak for the vapor jet, and both the V and L peaks for the liquid jet. We have included in the table a measurement for a RESS expansion that passes near the critical point between the vapor and liquid jet expansions; for this critical jet expansion, only the single dominant V type peak was resolved. Finally, for reference, we list a measurement for an expansion at a lower supercritical pressure (80 bar). As stated above, we feel our mean velocities are reliable within ∼1%, especially for the dominant peaks. However, our reported speed ratios are those deconvoluted and fit to the leading edge of the velocity distributions to avoid uncertainty due to space charge effects in the ionizer, so that they must be regarded as more qualitative.

To place these mean velocity data in perspective, an ideal gas calculation for CO_2 (assuming $\gamma = 1.4$) would predict terminal velocities of 673, 669, 654, and 673 m/s for the vapor jet, critical jet, liquid jet, and low-pressure jet expansions, respectively. Obviously these values are high compared to the experiments due to both the highly nonideal state of CO_2 in the stagnation region (with significant negative residual enthalpy) for these RESS expansions and the considerable condensation and fragmentation energy processes which may occur. We have analyzed the vapor jet expansion using the PR-EOS, coupled to an ideal gas equation of state for the later stages of the free-jet expansion[2] (see below), but neglecting clustering and condensation, and this more rigorous calculation predicts a terminal velocity of 445 m/s, compared to the measured 596 m/s. The difference is predominantly due to the heat released by condensation, which Khalil has shown can be substantial.[23] As we move to the lower pressure case (80 bar), where the nonideal gas effects and condensation effects are reduced, then we predict 592 m/s, which, as expected, is in better agreement with the measured 649 m/s value and also closer to the ideal gas limit.

TABLE 1: Summary of Time-of-Flight Velocity Distribution Measurements[a]

	P_o (bar)	T_o (K)	$V_{o,1}$ (m/s)	$V_{o,2}$ (m/s)	SR_1	SR_2
			vapor jet			
CO_2 (V)	140	343	596		39	
CO_2 (M)	140	343	687		6.5	
$(CO_2)_2$	140	343	696	604	15	34
$(CO_2)_3$	140	343	693		16	
$(CO_2)_4$	140	343	694		19	
$(CO_2)_5$	140	343	685		18	
$(CO_2)_6$	140	343	685		17	
$(CO_2)_7$	140	343	697		20	
$(CO_2)_8$	140	343	696		NA	
naphthalene	140	343	592		33	
			liquid jet			
CO_2 (V, L)	140	323	544	433	32	10
CO_2 (M)	140	323	∼630		NA	
$(CO_2)_2$	140	323	633	559	13	31
$(CO_2)_3$	140	323	631		12	
$(CO_2)_4$	140	323	628		15	
$(CO_2)_5$	140	323	630		13	
$(CO_2)_6$	140	323	637		22	
$(CO_2)_7$	140	323	620		13	
$(CO_2)_8$	140	323	612		12	
naphthalene	140	323	423		12	
$Fe(acac)_3$	140	323	∼435		∼8	
			critical jet			
CO_2	140	338	554		26	
			low P jet			
CO_2	80	343	649		31	

[a] Two mean velocities (V_o) and two speed ratios (SR) are reported for cases where multiple peaks are detected; see text for details.

3.E. Total Cross-Section Measurements. Subsequent to our velocity distribution measurements, we have made some preliminary total scattering cross-section measurements which support the explanation that the V and L peaks represent very large clusters reflected by monomer ion signals. The background density, n, in the buffer chamber housing the chopper (see Figure 2) was increased with Ar and the modulated beam signal for the monomer was monitored. Applying Beer's law, $I/I_o = \exp(-n\sigma L)$, to describe the attenuation we are able to extract an approximation to the total scattering cross section, σ. The experiment was not optimized for total cross-section measurements and has an angular resolution for the detector of ∼0.12° measured from the center of the scattering chamber, and a scattering path length of 18 cm. The data cannot be considered quantitative at this point since we have not made the type of corrections necessary, accounting for the distribution of relative velocities, integrating along the scattering path, and applying

quantum corrections for scattered particles reaching the detector.[45,46] However, when we calibrated with Ar beams, we deduce an Ar−Ar total cross section of ~280 Å^2 while the true total cross section in this energy range is of order 300 Å^2.[45] Although the experiment likely yields low total cross sections, the striking result is that the monomer attenuation yields impossibly low cross sections on the order of 1 Å^2 for both the vapor and liquid jet RESS expansion conditions. If we then lower the nozzle source pressure so that we have a low-pressure ideal gas CO_2 beam we measure a monomer cross section of ~210 Å^2, similar in magnitude to that for Ar. This qualitative scattering result indicates that the monomer ion signals observed in the V and L peaks in the high-pressure RESS expansions are in fact due to very large clusters, large enough that the Ar scattering is not able to deflect the massive particles from the detector. For example, a classical elastic scattering estimate of how large a cluster would need to be to avoid the detector acceptance angle, assuming the maximum momentum exchange normal to the beam axis, yields an estimate of order $N \approx 1000$. The scattering data are not reported here in any detail but they clearly support the explanation that the V and L peaks contain very large clusters which give rise to the large monomer ion signals due to electron beam fragmentation.

4. Analyses and Discussion

The velocity distribution data are provocative and certainly deserving of much further research beyond this study. A first glance at the experimental data might suggest that the CO_2 monomer fluid is primarily in the dominant V and L peaks, but this is not supported by the scattering data, previous studies in this field, nor the analyses discussed below. The V and L peaks are representative of very large condensed phase clusters and the monomer fluid is primarily reflected in the faster M peak.[47] The liquid jet, which undergoes fragmentation from a superheated state, is particularly interesting because of the large velocity slip between the two condensed cluster phases and the dramatic tendency of the solutes to remain only within the slower condensed phase, which we suggest is derived from the initial liquid phase fragment. The molecular dynamic simulations of Blink and Hoover[30] did indicate considerable variability in the fragment energies as a function of particle size for the fragmentation process, which could be the genesis of the large velocity slip between the V and L peaks. Knuth and others have made some progress in understanding analogous experiments for liquid helium expansions subject to fragmentation[28,48] and they were able to correlate their cluster distributions using the ideas of Grady[29] which minimize the sum of the kinetic energies of clusters relative to their center of mass and surface energies relative to the cluster surface areas. They observed multiple velocity peaks, detected as monomer He ions, and also showed that their large and slower peak was due to fragmentation of larger clusters. The helium data they use are much more comprehensive than our CO_2 data and, in particular, the helium expansion for very low temperature sources generated much larger clusters than we have observed and which are more amenable to the theoretical models. Henne and others[16,28,32,48] used a retarding field analyzer to detect clusters as large as 2×10^5. Certainly any continuum analysis of the expansion fluid mechanics and thermodynamics and near equilibrium modeling such as classical nucleation theories would predict very large clusters or condensed phase particles for our CO_2 RESS expansion. Khalil[23] completed preliminary calculations based on classical nucleation theories and showed that the condensation must be coupled directly into the rigorous continuum fluid mechanics calculations for the RESS expansion.

We provide some simplified analyses in the sections below, based on our velocity measurements, which can suggest limits on the underlying processes. These simplified calculations will also help direct future research and theoretical modeling of these complicated expansion processes.

4.A. Speed Ratio Scaling. As we have discussed above, the measured speed ratio for a cluster particle of mass N^*m is related to the local translational temperature in the jet by the following: $(SR_N)^2 = N^*m^*V^2/(2kT)$. If T is assumed, this relation can provide an estimate for $N = 2kT(SR_N)^2/(mV^2)$. We have measured SR and V, and we know m for CO_2, so we can use this relation in two ways: (1) assume T_N for the clusters is nearly the same as that measured for the monomer measurements, T_1, and predict N, or (2) assume a cluster size N and predict what T_N is characteristic of the cluster component in the expansion. For example, if we take the results for our vapor jet and assume the M peak represents monomers with $V_1 \approx 687$ m/s and $SR_1 \approx 6.5$ then we find a monomer fluid translational temperature of ~29 K. Considering the largest cluster in the vapor jet C peaks for which we have data, $N = 7$, we would predict a translational temperature of ~23 K, which is reasonably consistent. If we now assume thermal equilibrium between the M and V peak species, and take $T_N \approx T_1 \approx 25$ K and $S_N \sim 39$ and $V_N \sim 596$ m/s for the V peak, then we would predict that $N \approx 47$ would be typical of the V peak clusters.

However, as suggested above and by our analysis below, we feel that the V peak contains much larger clusters, in which case the velocity and speed ratio data will predict much higher local translational temperatures. For example, if the V peak clusters have N in the range 10^3 to 10^4 then the measured speed ratios (~40) would predict $T_N \approx 620$ to 6200 K for such large vapor jet clusters, and similarly large translational temperatures for the liquid jet condensed phase clusters. While high cluster temperatures for these expansions of superheated and supercooled fluids might be expected, such excessively high temperatures are not reasonable. To obtain more reasonable heated translational temperatures for the large V clusters, e.g. of order 100 K, would require speed ratios of order 100 and 300 for $N = 10^3$ and 10^4, respectively. We feel our deconvoluted tof experiments could measure speed ratios up to 100 but we did not see any indication of this for the V and L velocity distributions. A reasonable explanation for this inconsistency in the measured widths of the V and L velocity distributions is that these V and L peaks represent a distribution of very large clusters with a distribution of velocity slip and higher speed ratios, discussed further below.

4.B. Energy Balance Estimates. An energy balance for the adiabatic expansion takes the following rigorous form: $H_o(T_o,P_o) = \sum H_i(T,P) + \sum M_i V_i^2/2$, where the sum is over all cluster species, including monomer CO_2. The enthalpies include the internal vibrational states because these modes can participate to a small degree in the expansion and could be excited in the condensation or fragmentation processes. For our conditions, only the degenerate $\nu_2 = \nu_3$ vibration modes of molecular CO_2 are excited and only 6% and 5% are in the first excited state for our vapor and liquid expansions, respectively. A vibrational relaxation analysis for these modes[23,49] suggests that the vibrational energy is frozen out within two nozzle diameters of the sonic exit of the nozzle where only ~5% of the stagnation vibration energy has relaxed. We include this analysis in our simplified energy balance analysis below, although we do not account for additional excitation of internal energy that may be a result of the cluster formation kinetics.

We now construct a very simplified two-particle model for the vapor jet expansion and make the assumptions that we have only monomer CO_2 species and one large condensed phase species of average size N^*, that the difference in enthalpies between phases is a latent heat, characterized by λ per unit mass, and that the condensed phase and monomers are sufficiently cold so that we can neglect individual thermal enthalpies compared to the mean kinetic energies, with the exception of the CO_2 molecular vibrational energy. It is then straightforward to derive a very simplified energy balance:

$$H_o(T_o,P_o) - H^*_{vib} = (1-\omega)V_1^2/2 + \omega V_N^2/2 - \omega\lambda \quad (1)$$

where H^*_{vib} is the predicted residual molecular vibrational energy and the balance has been divided by total mass. Each term is on a per unit mass basis, and ω is the mass fraction of the condensed phase particle of average of size N^*. Assuming the V peak is predominantly the condensed phase and the M peak is predominantly the monomer phase, and taking $\lambda \approx 571$ kJ/kg (the heat of fusion of CO_2 at the triple point), we find that our velocity data for the vapor jet gives $\omega \approx 0.24$; approximately 24% of the vapor jet mass is predicted to have condensed to form a representative cluster N^* and assigned as the V peak in our tof data. It is useful to remember that mass fraction is related to number or mole fraction by the particle mass ratios, dependent on N, so that such a large mass fraction is contained in many fewer particles than the monomer species we observe.

Applying such an energy balance to the liquid jet expansion is even less straightforward because there are clearly more than two types of condensed species and we can expect substantial internal energy in the large particles formed from the fragmentation of the superheated liquid. There are several conceptual models to evaluate and we can only solve for one unknown parameter. However, as an example, if we assume the V and L peaks represent two condensed phases and are of equal mass, $\omega/2$, while the monomer is again represented by the M peak, we find that $\omega \approx 0.49$. While the model is simplistic and there are too many unknown parameters, such as an average N^* and λ, to make the analysis quantitative, the energy balance is one of the constraining conditions on any theoretical modeling of these expansions and the associated condensation and fragmentation processes.

As a qualitative comparison, if we sum, with no corrections for fragmentation or detector efficiencies, the experimental mass fractions of clusters observed in the vapor jet detected with the TOF-MS (Figure 3), we obtain the values $\omega_{exp}(\text{vapor}) \approx 0.10$. This measured mass fraction is less than that predicted by the energy balance above, which is consistent with the expectation that our TOF measurements may not have detected some larger clusters. If we do a similar sum over the observed TOF cluster peaks for the liquid jet we would obtain a $\omega_{exp}(\text{liquid}) \approx 0.14$.

The mass fraction of condensed species can also be estimated by using an equilibrium thermodynamic computation on the $T-S$ diagram and assuming there is equilibrium between the vapor and liquid phases (expected to give a maximum ω).[44] Making this calculation at the vapor jet expansion spinodal crossing point we get $\omega_{equil} \approx 0.10$. This value is again of the same order but smaller than the mass fraction predicted from the energy balance but agrees qualitatively with experimental cluster measurements, which is likely fortuitous. A similar calculation applied to the liquid jet crossing the spinodal gives $\omega_{equil} \approx 0.62$, more consistent with the energy balance estimate of 0.49 above, but it is much higher than the mass fraction measured with the TOF-MS, again supporting the fact that we have not detected the large condensed phase clusters and particles.

4.C. Velocity Slip Analysis. Velocity slip is a term used in the free-jet literature to account for nonequilibrated mean velocities when a carrier fluid is accelerating slower and heavier gas species, due to insufficient momentum transfer on the molecular level in the rapid expansion to low densities. This is also referred to as translational relaxation in the classical free-jet molecular beam field.[8,10,15] The degree of velocity slip observed far out in these RESS expansions ($\sim 200x/d$), where the molecular beam sampling occurs, is surprising. Such a high density jet would have been expected to be able to maintain nearly equilibrium mean velocity momentum, via the high rate of molecular collisions in the jet expansion, except for highly disparate masses. It is certainly not yet clear what cluster species exist in these highly nonideal RESS expansions or why one condensed phase formed in a liquid jet fragmentation would be moving at substantially different speeds than the other, even if initially one fragment was ejected with locally ballistic energies.[30] We examine the resulting velocity slip by using particle drag calculations in the jet, asking the question if a large cluster is suddenly placed into the jet at some initial location with some initial velocity, is there sufficient momentum transfer to equilibrate the two species before it is sampled by the skimmer, in our case at 200 nozzle diameters. We have made a few such calculations with the simplifying assumption that the carrier species is the CO_2 monomer expansion and that the expansion and drag are decoupled so that the appropriate drag coefficients are estimated by using continuum expansion properties characteristic of our RESS CO_2 expansions.[2] To accomplish this calculation we first had to extend our free-jet expansion calculations[2,22] to very large distances, well beyond the spinodal points where the PR-EOS is no longer useful. This has been done by matching the PR-EOS expansion profiles for $T(x)$, $\rho(x)$, and $V(x)$ to an ideal gas equation of state. Details of this analysis are provided elsewhere[2] but for the vapor jet the transition is very smooth at $\sim$11 nozzle diameters, while for the liquid jet the transition is only an approximation; the PR-EOS failed earlier in the expansion for the liquid jet.

These extended free-jet expansion profiles were then used in the following velocity slip calculation. We considered the drag force acting on a large particle in such a flow by using the following particle momentum equation,[50,51] which was integrated along the free-jet expansion centerline to predict the terminal particle velocity, V_p:

$$m_p \frac{DV_p}{Dt} = m_p \frac{dV_p}{dx} V_p = \frac{6\pi r_p \mu}{C}(u - V_p) \quad (2)$$

where D/Dt is the substantial derivative giving the rate of change following the particle along the streamline; m_p, V_p, and r_p are the mass, velocity, and radius of the particle, u is the fluid velocity, μ is the fluid viscosity, and C is the slip correction factor, important near the end of the expansion at lower densities, given by:[51]

$$C = 1 + \mathrm{Kn}\left[\alpha + \beta \exp\left(-\frac{\gamma}{\mathrm{Kn}}\right)\right] \quad (3)$$

where Kn is the Knudsen number $\mathrm{Kn} = \lambda/r_p$, where λ is the mean free path of the fluid. The parameters α, β, and γ have the values $\alpha = 1.257$, $\beta = 0.40$, $\gamma = 1.10$.[51] As an example, we present the results for acceleration of clusters for the vapor jet. Qualitatively we expect similar slip to occur in the liquid jet since the density and acceleration levels are similar.

Figure 12 shows results of the slip calculation for particles of different masses, formed at the spinodal point in the expansion with near-zero velocity. The spinodal region was chosen as the

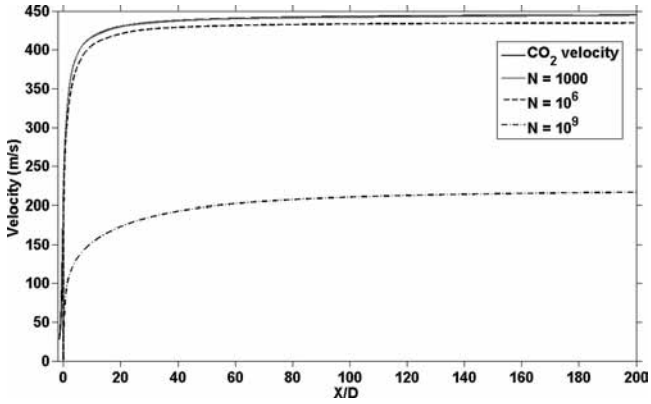

Figure 12. Acceleration of large particles formed at the spinodal with near zero velocity by CO_2 carrier fluid in a vapor jet expansion: P_o = 140 bar, T_o = 343 K; N = number of CO_2 monomer units in the particle.

starting point because that is the latest point in the expansion where the cluster formation or liquid fragmentation should begin.[26,27] The analysis shows that only very large particles present some velocity slip. In fact, a ~3 nm particle, composed of 1000 monomer units, has a negligible slip while a ~30 nm particle, with $N = 10^6$, is characterized by 2% slip. This result explains why all of the small clusters in the C peaks did not show significant velocity slip with respect to the monomer fluid. These slip calculations, even though they are decoupled and do not account for condensation, also support the conjecture that there are very large clusters in our RESS expansions, present in the V and the L peaks, which we have not been able to measure. Finally, since naphthalene has a mass equivalent to $N \approx 3$ it would be readily accelerated by the monomer fluid if it were not incorporated into the condensed phase early in the expansion or if it was subsequently evaporated from a condensed phase cluster. Therefore this result supports the conjecture that naphthalene is solvated within the condensed phases, consistent with thermodynamic expectations discussed above. Although not shown here, we have examined different starting locations upstream of the spinodal point for the large particles but there was little effect observed. Since fragmentation of superheated liquids can lead to locally ballistic velocities,[30] we have also examined and reported elsewhere the deceleration of large clusters[2] and found similar results for the size of particles required to exhibit such large velocity slip.

4.D. Summary. We have presented speed ratio, energy balance, and momentum drag analyses which support the conjecture that the large V and L peaks observed in these RESS expansions represent a distribution of very large condensed phase particles or clusters which are embedded in a monomer fluid phase. These large clusters are derived from the initial supercritical state by condensation of the vapor jet and fragmentation of the liquid jet. The data and analyses show that there is considerable momentum and thermal nonequilibrium throughout the RESS expansions between these highly disparate mass phases, clearly associated with the underling kinetic mechanisms responsible for their rapid formation. This conjecture is consistent with our total scattering cross-section measurements and with the existing literature on similar expansions of supercritical helium. Our analysis also supports the result that the low vapor pressure solutes remain within the condensed phase in which they are initially present, likely bound to a surrounding network of CO_2 molecules, and are not substantially present in the monomer fluid expansion. The smaller clusters which we are able to measure, and which are more nearly in equilibrium with the monomer fluid, are likely formed from the condensation of the interstitial monomer vapor during the free-jet expansion. The appearance of the major L peak when the superheated liquid jet undergoes fragmentation, and the clear association of low vapor pressure solutes with this L peak, is an important quantitative result worthy of additional theoretical analysis by molecular dynamic simulation.

It is more difficult to explain why we did not observe small clusters, other than the dimer, in the V and L peaks. Two possible explanations are that our signal-to-noise was not sufficient to identify them and/or the electron beam fragmentation process primarily yields the monomer ions and much fewer small cluster ions. This latter explanation is both interesting in itself and consistent with similar results found for the supercritical helium expansions.[31]

5. Conclusions

We have been able to couple high-density RESS expansions of supercritical CO_2, with and without solutes, to a mass spectrometer apparatus. We identified solvent cluster species and made velocity distribution measurements of the near terminal states of these expansions. The major result is that when we expand a liquid jet we observe two dominant, nonequilibrated, velocity peaks which must be associated with an energetic fragmentation process of the superheated liquid state. This result of multiple velocity peaks is qualitatively similar to those of Knuth, Toennies, and colleagues[12,26,31] for helium expansions. However, by adding solutes we have been able to tag one of the velocity peaks to a unique slower component of the fragmentation process for superheated liquids, which we suggest is the condensed phase fragmentation particle initially associated with the liquid phase component. We have made qualitative total scattering measurements and provided analyses to show that the two dominant velocity peaks are both associated with very large condensed phase clusters. We are not able to offer an analysis of the processes responsible for these results, which must come from molecular dynamics simulations. We would suggest, given the rapid microsecond scale for the decompression time which suggests little likelihood of any molecular transport of heat to or from nucleating bubbles or clusters, that the type of models explored by Grady[29] and Hoover[30] will be the most applicable. We also find small CO_2 cluster species moving together with the primary monomer fluid, but faster than the dominant condensed phase peaks in both vapor and liquid jets. We plan to introduce repelling grid type mass discrimination and possibly light scattering to characterize the very large nanoscale clusters which our present analysis suggest and which our present mass spectrometers are not able to detect. The possibility of spatially separating the different components by tof beam modulation could be an important experimental advantage. These future experiments could help us understand the substantial translational nonequilibrium, related to molecular dynamics, observed for both supersaturated vapor jets and superheated liquid jets.

Acknowledgment. This work was partially supported by National Science Foundation grant CHE-0136195. We thank Dr. Morton Fineman and Professor Eldon Knuth for helpful discussions.

References and Notes

(1) De Dea, S.; Graziani, D.; Miller, D. R.; Continetti, R. E. *J. Supercrit. Fluids* **2007**, *42*, 410.

(2) De Dea, S. Nano-scale Magnetic Film Formation by Decompression of Supercritical CO_2/Ferric Acetylacetonate Solutions, Ph.D. Thesis, University of California, San Diego, 2008.
(3) Petersen, R. C.; Matson, D. W.; Smith, R. D. *J. Am. Chem. Soc.* **1986**, *108*, 2100.
(4) Tom, J. W.; Debenedetti, P. G. *J. Aerosol Sci.* **1991**, *22*, 555.
(5) Weber, M.; Thies, M. Understanding the RESS process. In *Supercritical fluid technology in materials science and engineering*; Sun, Y., Ed.; Marcel Dekker: New York, 2002; p 387.
(6) Maharrey, S. P.; Miller, D. R. *J. Phys. Chem. A* **2001**, *105*, 5860.
(7) Anderson, J. B. Molecular Beams from Nozzle Sources. In *Molecular Beams and Low Density Gasdynamics*; Wagener, P. P., Ed.; Marcel Dekker, Inc: New York, 1974.
(8) Miller, D. R. Free Jet Sources. In *Atomic and Molecular Beam Methods*; Scoles, G., Ed.; Oxford University Press: New York, 1988; Vol. 1, p 14.
(9) Scoles, G. *Atomic and Molecular Beam Methods*; Oxford University Press: New York, 1988; Vol. 12.
(10) Campargue, R. *Atomic and Molecular Beams: The State of the Art 2000*; Springer-Verlag: New York,2001.
(11) Ekinci, Y.; Knuth, E. L.; Toennies, J. P. *J. Chem. Phys.* **2006**, 125.
(12) Knuth, E. L.; Schunemann, F.; Toennies, J. P. *J. Chem. Phys.* **1995**, *102*, 6258.
(13) Wormer, P. E. S.; van der Avoird, A. *Chem. Rev.* **2000**, *100*, 4109.
(14) Hillenkamp, M.; Keinan, S.; Even, U. *J. Chem. Phys.* **2003**, *118*, 8699.
(15) Schwartz, M. H.; Andres, R. P. *J. Aerosol Sci.* **1976**, *7*, 281.
(16) Hagena, O. F. Cluster beams from nozzle sources. In *Molecular beams and low density gasdynamics*; Wagener, P. P., Ed.; Marcel Dekker, Inc: New York, 1974.
(17) Hagena, O. F. *Z. Phys. D: At., Mol. Clusters* **1987**, *4*, 291.
(18) Montero, S.; Tejeda, B. M. G.; Fernandez, J. M.; Ramos, A. Raman Studies of Free-Jet Expansion (Diagnostic and Mapping). In *Atomic and Molecular Beams: the State of the Art 2000*; Campargue, R., Ed.; Springer-Verlag: New York,2001.
(19) Bonnamy, A.; Hermsdorf, D.; Ueberschaer, R.; Signorell, R. *Rev. Sci. Instrum.* **2005**, 76.
(20) Christen, W.; Geggier, S.; Grigorenko, S.; Rademann, K. *Rev. Sci. Instrum.* **2004**, *75*, 5048.
(21) Zhang, Q.; Wodtke, A. M. *Anal. Chem.* **2005**, *77*, 7612.
(22) Khalil, I.; Miller, D. R. *AIChE J.* **2004**, *50*, 2697.
(23) Khalil, I. Free-Jet Expansion of Supercritical CO_2, Ph.D. Thesis, University of California, San Diego, 2003.
(24) Christen, W.; Rademann, K. *Phys. Rev. A* **2008**, 77.
(25) Span, R.; Wagner, W. *J. Phys. Chem. Ref. Data* **1996**, *25*, 1509.
(26) Harms, J.; Toennies, J. P.; Knuth, E. L. *J. Chem. Phys.* **1997**, *106*, 3348.
(27) Holian, B. L.; Grady, D. E. *Phys. Rev. Lett.* **1988**, *60*, 1355.
(28) Knuth, E. L.; Henne, U. *J. Chem. Phys.* **1999**, *110*, 2664.
(29) Grady, D. E. *J. Appl. Phys.* **1982**, *53*, 322.
(30) Blink, J. A.; Hoover, W. G. *Phys. Rev. A* **1985**, *32*, 1027.
(31) Buchenau, H.; Knuth, E. L.; Northby, J.; Toennies, J. P.; Winkler, C. *J. Chem. Phys.* **1990**, *92*, 6875.
(32) Northby, J. A. *J. Chem. Phys.* **2001**, *115*, 10065.
(33) Debenedetti, P. G. *Metastable Liquids. Concepts and Principles*; Princeton University Press: Princeton, NJ, 1996.
(34) Fowles, G. R. *Vapor detonations in superheated fluids*, IUTAM symposium, 1989, Gottingen/Germany.
(35) Campargue, R. *J. Phys. Chem.* **1984**, *88*, 4466.
(36) Wiley, W. C.; McLaren, I. H. *Rev. Sci. Instrum.* **1955**, *26*, 1150.
(37) Cotter, R. J. *Time-Of-Flight Mass Spectrometry*; ACS Symp. Ser., No. 549; American Chemical Society: Washington, DC, 1994.
(38) Andrews, L.; Rohrbacher, A.; Laperle, C. M.; Continetti, R. E. *J. Phys. Chem. A* **2000**, *104*, 8173.
(39) Hagena, O. F.; Varma, A. K. *Rev. Sci. Instrum.* **1968**, *39*, 47.
(40) Alcalay, J. A.; Knuth, E. L. *Rev. Sci. Instrum.* **1969**, *40*, 438.
(41) Echt, O.; Kandler, O.; Leisner, T.; Miehle, W.; Recknagel, E. *J. Chem. Soc., Faraday Trans.* **1990**, *86*, 2411.
(42) Friedman, L.; Beuhler, R. J. *J. Chem. Phys.* **1983**, *78*, 4669.
(43) Christen, W.; Rademann, K.; Even, U. *J. Chem. Phys.* **2006**, 125.
(44) Sandler, S. I. *Chemical and Engineering Thermodynamics*; John Wiley: Hoboken, NJ,, 1999.
(45) Nenner, T.; Tien, H.; Fenn, J. B. *J. Chem. Phys.* **1975**, *63*, 5439.
(46) Demartino, A.; Benslimane, M.; Chatelet, M.; Crozes, C.; Pradere, F.; Vach, H. *Z. Phys. D: At., Mol. Clusters* **1993**, *27*, 185.
(47) Knuth, E., private communication; the authors are indebted to Professor Knuth for his insight and suggestion to consider this explanation.
(48) Jiang, T.; Northby, J. A. *Phys. Rev. Lett.* **1992**, *68*, 2620.
(49) Hecht, C. E. *Statistical Thermodynamics and Kinetic Theory*; Dover Publications, Inc: Mineola, NY, 1990.
(50) Williams, M. M. R.; Loyalka, S. K. *Aerosol Science: Theory and Practice with Special Applications to the Nuclear Industry*; Pergamon Press: New York, 1991.
(51) Flagan, R. C.; Seinfeld, J. H. *Fundamentals of air pollution engineering*; Prentice Hall: Upper Saddle River, NJ, 1988.

JP805618Z